

The relativistic eikonal approximation in high-energy $A(e, e'p)$ reactions

D. Debruyne, J. Ryckebusch, W. Van Nespén and S. Janssen
Department of Subatomic and Radiation Physics,
Ghent University, Proeftuinstraat 86, B-9000 Gent, Belgium
(November 28, 2018)

A fully relativistic model for the description of exclusive $(e, e'p)$ reactions off nuclear targets at high energies and momentum transfers is outlined. It is based on the eikonal approximation for the ejectile scattering wave function and a relativistic mean-field approximation to the Walecka model. Results for $^{12}\text{C}(e, e'p)$ and $^{16}\text{O}(e, e'p)$ differential cross sections and separated structure functions are presented for four-momenta in the range $0.8 \leq Q^2 \leq 20$ $(\text{GeV}/c)^2$. The regions of applicability of the eikonal approximation are studied and observed to be confined to proton knockout in a relatively small cone about the momentum transfer. A simple criterium defining the boundaries of this cone is determined. The Q^2 dependence of the effect of off-shell ambiguities on the different $(e, e'p)$ structure functions is addressed. At sufficiently high values of Q^2 their impact on the cross sections is illustrated to become practically negligible. It is pointed out that for the whole range of Q^2 values studied here, the bulk of the relativistic effects arising from the coupling between the lower components in the wave functions, is manifesting itself in the longitudinal-transverse interference term.

PACS: 24.10.-i, 24.10.Jv, 25.30.Fj

Keywords : Relativistic Eikonal Approximation, Exclusive $(e, e'p)$ reactions.

I. INTRODUCTION

Exclusive $A(e, e'p)B$ reactions from nuclei constitute an invaluable tool to probe a wide variety of nuclear phenomena. At low values of the virtual photon's four-momentum transfer $Q^2 = \vec{q}^2 - \omega^2$ and, accordingly, larger distance scales, the quasi-elastic $A(e, e'p)$ reaction probes the mean-field structure of nuclei. From systematic investigations for a large number of target nuclei a richness of precise information about the independent-particle wave functions and spectroscopic strengths was assembled [1]. At high Q^2 and decreasing distance scales, the scope of exclusive $(e, e'p)$ measurements shifts towards studies of (possible) medium dependencies of the nucleonic properties, and, effects like color transparency and the short-range structure of nuclei. Within the context of exclusive $(e, e'p)$ reactions, “color transparency” stands for the suggestion that at sufficiently high values of Q^2 the struck proton may interact in an anomalously weak manner with the “spectator” nucleons in the target nucleus [2].

The extraction of physical information from measured $A(e, e'p)B$ cross sections usually involves some theoretical modelling of which the major ingredients are the initial (bound) and final (scattering) proton wave functions and the electromagnetic electron-nucleus coupling. At lower values of Q^2 , most theoretical work on $(e, e'p)$ reactions was performed in the so-called distorted-wave impulse approximation (DWIA). The idea behind the DWIA approach is that the initial (bound) and final (scattering) state of the struck nucleon can be computed in a potential model, whereas for the electron-nucleus coupling an “off-shell corrected” electron-proton form can be used. The wealth of high-quality $(e, e'p)$ data that electron-scattering experiments have provided over the last 20 years, made sure that the DWIA models are well tested against experimental data. For higher values of the energy and momentum transfer ($Q^2 \gtrsim 1$ $(\text{GeV}/c)^2$), most theoretical $(e, e'p)$ work starts from the non-relativistic Glauber theory [3]. This theory is highly successful in describing small angle proton-nucleus scattering at higher energies [4] and is conceived as a baseline for calculating the effect of final-state interactions in high-energy $(e, e'p)$ reactions. Glauber theory is a multiple-scattering extension of the standard eikonal approximation that relates through a profile function the ejectile's distorted wave function to the elastic proton scattering wave function [3,5–8]. The Glauber method has frequently been shown to be reliable in describing $A(p, p')$ processes. Several non-relativistic studies [9–11] have formally investigated the applicability of the Glauber model for describing $A(e, e'p)$ reactions at higher energies and momentum transfers. Recently, the first high-quality data for exclusive $^{16}\text{O}(e, e'p)$ cross sections at higher four-momentum transfer ($Q^2 \geq 1$ $(\text{GeV}/c)^2$) became available [12]. Below, we will compare results of relativistic eikonal calculations with these data. We believe that this comparison between model calculations and data provides a stringent test of the applicability of the eikonal approximation in describing $(e, e'p)$ reactions.

Since relativistic effects are expected to become critical in the GeV energy domain, we explore the possibility of developing a fully relativistic model for $A(e, e'p)$ processes, thereby using the eikonal limit to solve the equations for the final-state wave functions. We employ a relativistic mean-field approximation to the Walecka model to determine

the bound state wave functions and binding energies, as well as nucleon and meson potentials. The same mean-field potentials are then also used to compute the scattering wave function in the Dirac eikonal limit. The work presented here is a small initial step towards the formulation of a fully microscopic relativistic model for the description of $(e, e'p)$ reactions that could possibly bridge the gap between the low and intermediate-energy regime. The model developed in this work can be formally applied in a wide Q^2 range. As a matter of fact, we employ the relativistic eikonal method to estimate the sensitivity of $(e, e'p)$ observables in the few GeV regime to a number of physical effects, including off-shell ambiguities and relativity. We adopt different prescriptions for the electron-nucleus coupling in our calculations. By doing this, we estimate the sensitivity of the observables to the theoretical uncertainties that surround the choice of the off-shell electron-proton vertex. It is often claimed that off-shell ambiguities decrease in importance as the four-momentum transfer increases. Here, we make an attempt to quantify the relative importance of the off-shell effects for the $(e, e'p)$ structure functions by comparing results obtained with different off-shell electron-proton couplings. Hereby we are primarily concerned with the question how big the uncertainties remain when higher and higher four-momentum transfers are probed.

In Sect. II we introduce a relativistic eikonal formalism for calculating $A(e, e'p)$ observables. This includes a discussion of the method employed to determine the bound (Sect. II B) and scattering (Sect. II C) states. Various forms for the photon-nucleus interaction vertex are introduced in Sect. II D, where special attention is paid to the issue of current conservation. In Sect. III we present the results of our $^{12}\text{C}(e, e'p)$ and $^{16}\text{O}(e, e'p)$ numerical calculations. In Sect. III B we focus on the issue of the Q^2 evolution of the off-shell ambiguities. In Sect. III C we compare the results of a fully relativistic calculation with a calculation in which the explicit coupling between the lower components in the initial and final state are neglected. Finally, our concluding remarks are summarized in Sect. IV.

II. FORMALISM

A. Reaction observables and kinematics.

In this work we follow the conventions for the $(\vec{e}, e'\vec{p})$ kinematics and observables introduced by Donnelly and Raskin in Ref. [13]. The four-momenta of the incident and scattered electrons are labeled as $K^\mu(\epsilon, \vec{k})$ and $K'^\mu(\epsilon', \vec{k}')$. The electron momenta \vec{k} and \vec{k}' define the scattering plane. The four-momentum transfer is given by $q^\mu = K^\mu - K'^\mu = P_{A-1}^\mu + P_f^\mu - P_A^\mu$, where P_A^μ and P_{A-1}^μ are the four-momenta of the target and residual nucleus, while P_f^μ is the four-momentum of the ejected nucleon. Also, $q^\mu = (\omega, \vec{q})$, where the three-momentum transfer $\vec{q} = \vec{k} - \vec{k}' = \vec{k}_{A-1} + \vec{k}_f - \vec{k}_A$ and the energy transfer $\omega = \epsilon - \epsilon' = E_{A-1} + E_f - E_A$ are defined in the standard manner. The xyz coordinate system is chosen such that the z -axis lies along the momentum transfer \vec{q} , the y -axis lies along $\vec{k} \times \vec{k}'$ and the x -axis lies in the scattering plane; the reaction plane is then defined by \vec{k}_f and \vec{q} . The Bjorken-Drell convention [14] for the gamma matrices and Dirac spinors is followed, so that the normalization condition for Dirac plane waves, characterized by a four-momentum K^μ and spin-state S^μ , is $\bar{u}(K^\mu, S^\mu)u(K^\mu, S^\mu) = 1$.

In the one-photon-exchange approximation, the process in which a longitudinally polarized electron with helicity h , impinges on a nucleus and induces the knockout of a single nucleon, leaving the residual nucleus in a certain discrete state, can be written in the following form [13]:

$$\frac{d^5\sigma}{d\epsilon' d\Omega_{e'} d\Omega_x} = \frac{MM_{A-1}k_f}{8\pi^3 M_A} f_{rec}^{-1} \sigma_M \left[(v_L \mathcal{R}_L + v_T \mathcal{R}_T + v_{TT} \mathcal{R}_{TT} + v_{TL} \mathcal{R}_{TL}) + h(v_{T'} \mathcal{R}_{T'} + v_{TL'} \mathcal{R}_{TL'}) \right], \quad (1)$$

where f_{rec} is the hadronic recoil factor

$$f_{rec} = \frac{E_{A-1}}{E_A} \left| 1 + \frac{E_f}{E_{A-1}} \left(1 - \frac{\vec{q} \cdot \vec{k}_f}{k_f^2} \right) \right| = \left| 1 + \frac{\omega k_f - E_f q \cos \theta_f}{M_A k_f} \right|, \quad (2)$$

with θ_f the angle between \vec{k}_f and \vec{q} , and σ_M the Mott cross section

$$\sigma_M = \left(\frac{\alpha \cos \theta_e / 2}{2\epsilon \sin^2 \theta_e / 2} \right)^2, \quad (3)$$

with θ_e the angle between the incident and the scattered electron. The electron kinematics is contained in the kinematical factors

$$v_L = \left(\frac{Q^2}{q^2} \right)^2, \quad (4)$$

$$v_T = -\frac{1}{2} \left(\frac{Q^2}{q^2} \right) + \tan^2 \frac{\theta_e}{2}, \quad (5)$$

$$v_{TT} = \frac{1}{2} \left(\frac{Q^2}{q^2} \right), \quad (6)$$

$$v_{TL} = \frac{1}{\sqrt{2}} \left(\frac{Q^2}{q^2} \right) \sqrt{-\left(\frac{Q^2}{q^2} \right) + \tan^2 \frac{\theta_e}{2}}, \quad (7)$$

$$v_{T'} = \tan \frac{\theta_e}{2} \sqrt{-\left(\frac{Q^2}{q^2} \right) + \tan^2 \frac{\theta_e}{2}}, \quad (8)$$

$$v_{TL'} = \frac{1}{\sqrt{2}} \left(\frac{Q^2}{q^2} \right) \tan \frac{\theta_e}{2}, \quad (9)$$

whereas the structure functions are defined in a standard fashion as

$$\mathcal{R}_L = |\rho(\vec{q})_{fi}|^2, \quad (10)$$

$$\mathcal{R}_T = |J(\vec{q}; +1)_{fi}|^2 + |J(\vec{q}; -1)_{fi}|^2, \quad (11)$$

$$\mathcal{R}_{TT} = 2 \operatorname{Re} \{ J^*(\vec{q}; +1)_{fi} J(\vec{q}; -1)_{fi} \}, \quad (12)$$

$$\mathcal{R}_{TL} = -2 \operatorname{Re} \{ \rho^*(\vec{q})_{fi} (J(\vec{q}; +1)_{fi} - J(\vec{q}; -1)_{fi}) \}, \quad (13)$$

$$\mathcal{R}_{T'} = |J(\vec{q}; +1)_{fi}|^2 - |J(\vec{q}; -1)_{fi}|^2, \quad (14)$$

$$\mathcal{R}_{TL'} = -2 \operatorname{Re} \{ \rho^*(\vec{q})_{fi} (J(\vec{q}; +1)_{fi} + J(\vec{q}; -1)_{fi}) \}, \quad (15)$$

where $\rho(\vec{q})_{fi}$ is the transition charge density, while $J(\vec{q}; m = \pm 1)_{fi}$ is the transition three-current expanded in terms of the standard spherical components.

B. Bound state wave functions.

A relativistic quantum field theory for nucleons (ψ) interacting with scalar mesons (ϕ) through a Yukawa coupling $\bar{\psi}\psi\phi$ and with neutral vector mesons (V_μ) that couple to the conserved baryon current $\bar{\psi}\gamma_\mu\psi$, can be described through a lagrangian density of the type [15,16]

$$\begin{aligned} \mathcal{L}_0 = & \bar{\psi}(\imath\partial - M)\psi + \frac{1}{2}(\partial_\mu\phi\partial^\mu\phi - m_s^2\phi^2) - \frac{1}{4}G_{\mu\nu}G^{\mu\nu} \\ & + \frac{1}{2}m_v^2V_\mu V^\mu - g_v\bar{\psi}\gamma_\mu\psi V^\mu + g_s\bar{\psi}\psi\phi, \end{aligned} \quad (16)$$

with M , m_s and m_v the nucleon, scalar meson and vector meson masses, respectively, and $G^{\mu\nu} \equiv \partial^\mu V^\nu - \partial^\nu V^\mu$ the vector meson field strength. The scalar and vector fields may be associated with the σ and ω mesons. The model can be extended to include also π and ρ mesons, as well as the coupling to the photon field. The corresponding lagrangian has the form

$$\begin{aligned} \mathcal{L} = & \mathcal{L}_0 + \frac{1}{2}(\partial_\mu\vec{\pi} \cdot \partial^\mu\vec{\pi} - m_\pi^2\vec{\pi} \cdot \vec{\pi}) - \imath g_\pi\bar{\psi}\gamma_5\vec{\tau} \cdot \vec{\pi}\psi - \frac{1}{4}\vec{B}_{\mu\nu} \cdot \vec{B}^{\mu\nu} \\ & + \frac{1}{2}m_\rho^2\vec{b}_\mu \cdot \vec{b}^\mu - \frac{1}{2}g_\rho\bar{\psi}\gamma_\mu\vec{\tau} \cdot \vec{b}^\mu\psi - \frac{1}{4}F_{\mu\nu}F^{\mu\nu} \\ & - eA_\mu[\bar{\psi}\gamma^\mu\frac{1}{2}(1 + \tau_3)\psi + (\vec{b}_\nu \times \vec{B}^{\nu\mu})_3 + (\vec{\pi} \times (\partial^\mu\vec{\pi} + g_\rho(\vec{\pi} \times \vec{b}^\mu))]_3]. \end{aligned} \quad (17)$$

Here $\vec{\pi}$, \vec{b}_μ , A_μ , $F_{\mu\nu}$ are the pion, rho, Maxwell and electromagnetic fields. Further, $\vec{B}^{\mu\nu} \equiv \partial^\mu\vec{b}^\nu - \partial^\nu\vec{b}^\mu - g_\rho(\vec{b}^\mu \times \vec{b}^\nu)$ is the ρ -meson field.

At sufficiently high densities, the meson field operators can be approximated by their expectation values. Within the context of the relativistic Hartree approximation, it can be shown that when starting from the lagrangian (17) the following Dirac equation for the baryon field Ψ results [16] :

$$[i\gamma^\mu \partial_\mu - M - \Sigma_H] \Psi = 0, \quad (18)$$

where the self-energy Σ_H is defined as

$$\Sigma_H = -g_s \phi + g_v \gamma_\mu V^\mu + g_\pi \gamma_5 \tau_\alpha \pi^\alpha + \frac{1}{2} g_\rho \gamma_\mu \tau_\alpha b^{\mu\alpha} + \frac{1}{2} \gamma_\mu (1 + \tau_3) A^\mu. \quad (19)$$

Assuming that the nuclear ground state is spherically symmetric and a parity eigenstate, it can be shown that the pion field does not enter in the Hartree approximation. Furthermore, the meson fields only depend on the radius, and only the time component of the vector fields contribute. The time-independent Dirac equation can then be written as :

$$\hat{H}\Psi(\vec{x}) \equiv \left[-i\vec{\alpha} \cdot \vec{\nabla} + g_v V^0(r) + \frac{1}{2} g_\rho \tau_\alpha b^{0\alpha}(r) + \frac{1}{2} e(1 + \tau_3) A^0(r) + \gamma^0 (M - g_s \phi^0(r)) \right] = E\Psi(\vec{x}). \quad (20)$$

The general solutions to a Dirac equation with spherically symmetric potentials have the form

$$\psi_\alpha(\vec{x}) \equiv \psi_{n\kappa m t}(\vec{x}) = \begin{bmatrix} iG_{n\kappa t}(r)/r \mathcal{Y}_{\kappa m} \eta_t \\ -F_{n\kappa t}(r)/r \mathcal{Y}_{-\kappa m} \eta_t \end{bmatrix}, \quad (21)$$

where n denotes the principal, κ and m the generalized angular momentum and t the isospin quantum numbers. The $\mathcal{Y}_{\pm\kappa m}$ are the well-known spin spherical harmonics and determine the angular and spin parts of the wavefunction,

$$\mathcal{Y}_{\kappa m} = \sum_{m_l m_s} \langle l m_l \frac{1}{2} m_s | l \frac{1}{2} j m \rangle Y_{l, m_l} \chi_{\frac{1}{2} m_s},$$

$$j = |\kappa| - \frac{1}{2}, \quad l = \begin{cases} \kappa, & \kappa > 0 \\ -(\kappa + 1), & \kappa < 0. \end{cases} \quad (22)$$

The Hartree approximation leads to the following set of coupled equations for the different fields [16] :

$$\begin{aligned} \frac{d^2}{dr^2} \phi_0(r) + \frac{2}{r} \frac{d}{dr} \phi_0(r) - m_s^2 \phi_0(r) &= -g_s \rho_s(r) \\ &\equiv -g_s \sum_{\alpha_{occ}} \left(\frac{2J_\alpha + 1}{4\pi r^2} \right) (|G_\alpha(r)|^2 - |F_\alpha(r)|^2), \\ \frac{d^2}{dr^2} V_0(r) + \frac{2}{r} \frac{d}{dr} V_0(r) - m_v^2 V_0(r) &= -g_v \rho_B(r) \\ &\equiv -g_v \sum_{\alpha_{occ}} \left(\frac{2J_\alpha + 1}{4\pi r^2} \right) (|G_\alpha(r)|^2 + |F_\alpha(r)|^2), \\ \frac{d^2}{dr^2} b_0(r) + \frac{2}{r} \frac{d}{dr} b_0(r) - m_\rho^2 b_0(r) &= -\frac{1}{2} g_\rho \rho_3(r) \\ &\equiv -\frac{1}{2} g_\rho \sum_{\alpha_{occ}} \left(\frac{2J_\alpha + 1}{4\pi r^2} \right) (|G_\alpha(r)|^2 + |F_\alpha(r)|^2) (-1)^{t_\alpha - 1/2}, \\ \frac{d^2}{dr^2} A_0(r) + \frac{2}{r} \frac{d}{dr} A_0(r) &= -e \rho_P(r) \\ &\equiv -e \sum_{\alpha_{occ}} \left(\frac{2J_\alpha + 1}{4\pi r^2} \right) (|G_\alpha(r)|^2 + |F_\alpha(r)|^2) (t_\alpha + \frac{1}{2}), \\ \frac{d}{dr} G_\alpha(r) + \frac{\kappa}{r} G_\alpha(r) - [\epsilon_\alpha - g_v V_0(r) - t_\alpha g_\rho b_0(r) \\ &\quad - (t_\alpha + \frac{1}{2}) e A_0(r) + M - g_s \phi_0(r)] F_\alpha(r) = 0, \\ \frac{d}{dr} F_\alpha(r) - \frac{\kappa}{r} F_\alpha(r) + [\epsilon_\alpha - g_v V_0(r) - t_\alpha g_\rho b_0(r) \\ &\quad - (t_\alpha + \frac{1}{2}) e A_0(r) - M + g_s \phi_0(r)] G_\alpha(r) = 0, \\ \int_0^\infty dr (|G_\alpha|^2 + |F_\alpha|^2) &= 1. \end{aligned} \quad (23)$$

The above equations constitute the basis of the relativistic mean-field approach to the lagrangian of Eq. (17).

A new computer program to solve the above set of coupled non-linear differential equations was developed. Starting from an initial guess of the Woods-Saxon form for the scalar and vector potential, the Dirac equations can be solved iteratively using a shooting point method. Analytic solutions to the equations in the regions of large and small r allow to impose the proper boundary conditions. Once the nucleon wave functions are obtained, the densities and meson fields can be re-evaluated. This procedure is repeated a number of times until convergence for the energy eigenvalues is reached. We adopt the values for the σ , ω and ρ masses and coupling constants as they were introduced by Horowitz and Serot [16].

For the ^{12}C and ^{16}O nuclei, the newly developed C-code **SOR** performed all integrations for a radial extension of the nucleus of 20 fm and a stepsize of 0.01 fm. The coupled Dirac equations were solved for a shooting point lying at 2 fm using a fourth order Runge-Kutta algorithm. As a convergence criterium we imposed a tolerance level as small as 0.001 MeV on all single-particle energy levels. The computed densities for the nuclei ^{12}C and ^{16}O , are depicted in Fig. 1. We have verified that these results are comparable to those produced by the **TIMORA** code [16], which is widely used to solve the set of Eqs. (23).

C. The eikonal final state.

To construct the scattering states for the ejected nucleons, we consider the hamiltonian (20) that was already used to calculate the bound state wave functions

$$\hat{H} \equiv -i\vec{\alpha} \cdot \vec{\nabla} + \gamma^0 M + \gamma^0 \Sigma_H(r), \quad (24)$$

where the self-energy $\Sigma_H(r)$ is given by

$$\Sigma_H(r) = -g_s \phi_0(r) + g_v \gamma_0 V^0(r) + \frac{1}{2} g_\rho \gamma_0 \tau_\alpha b^{0\alpha}(r) + \frac{1}{2} e \gamma_0 (1 + \tau_3) A^0(r). \quad (25)$$

With the formal substitutions

$$\begin{aligned} V_s(r) &\equiv -g_s \phi_0, \\ V_v(r) &\equiv g_v V_0(r) + \frac{1}{2} g_\rho b_0(r) (-1)^{t_\alpha - 1/2} + e A_0(r) (t_\alpha + \frac{1}{2}), \end{aligned} \quad (26)$$

the time independent Dirac equation for a projectile with relativistic energy $E = \sqrt{k^2 + M^2}$ and spin state s , can be cast in the form

$$\hat{H} \phi_{\vec{k},s}^{(+)} = [\vec{\alpha} \cdot \vec{p} + \beta M + \beta V_s(r) + V_v(r)] \phi_{\vec{k},s}^{(+)}, \quad (27)$$

where we have introduced the notation $\phi_{\vec{k},s}^{(+)}$ for the unbound Dirac states. The computed scalar and vector potentials for the ^{12}C and ^{16}O nuclei are displayed in Fig. 2

After some straightforward manipulations, a Schrödinger-like equation for the upper component can be obtained

$$\left[\frac{p^2}{2M} + V_c + V_{so}(\vec{\sigma} \cdot \vec{L} - i\vec{r} \cdot \vec{p}) \right] u_{\vec{k},s}^{(+)} = \frac{k^2}{2M} u_{\vec{k},s}^{(+)}, \quad (28)$$

where the central and spin orbit potentials V_c and V_{so} are defined as

$$\begin{aligned} V_c(r) &= V_s(r) + \frac{E}{M} V_v(r) + \frac{V_s(r)^2 - V_v(r)^2}{2M}, \\ V_{so}(r) &= \frac{1}{2M[E + M + V_s(r) - V_v(r)]} \frac{1}{r} \frac{d}{dr} [V_s(r) - V_v(r)]. \end{aligned} \quad (29)$$

In computing the scattering wave functions, we use the scalar and vector potentials as obtained from the iterative bound state calculations. As a result the initial and final state wave functions are orthogonalized and no spurious contributions can be expected to enter the calculated cross sections.

Since the lower component is related to the upper one through

$$w_{\vec{k},s}^{(+)} = \frac{1}{E + M + V_s - V_v} \vec{\sigma} \cdot \vec{p} u_{\vec{k},s}^{(+)}, \quad (30)$$

the solutions to the equation (28) determine the complete relativistic eigenvalue problem. So far no approximations have been made. Various groups [17–19] have solved the Dirac equation (28) for the final scattering state using Dirac optical potentials derived from global fits to elastic proton scattering data [20]. Not only are global parametrizations of Dirac optical potentials usually restricted to proton kinetic energies $T_p \leq 1$ GeV, calculations based on exact solutions of the Dirac equation frequently become impractical at higher energies. This is particularly the case for approaches that rely on partial-wave expansions in determining the transition matrix elements. To overcome these complications, we solve the Dirac equation (28) in the eikonal limit [21,22]. In intermediate-energy proton scattering ($T_p \approx 500$ MeV) the eikonal approximation was shown to reproduce fairly well the exact Dirac partial wave results [23]. Following the discussion of Ref. [23], we define the average momentum \vec{K} and the momentum transfer \vec{q} in terms of the projected initial (\vec{k}_i) and final momentum (\vec{k}_f) of the ejectile

$$\vec{q} = \vec{k}_f - \vec{k}_i, \quad (31)$$

$$\vec{K} = \frac{1}{2}(\vec{k}_f + \vec{q}). \quad (32)$$

In the eikonal, or, equivalently, the small-angle approximation ($q \gg k_i$) the following operatorial substitution is made in computing the scattering wave function

$$p^2 = [(\vec{p} - \vec{K}) + \vec{K}]^2 \longrightarrow 2\vec{K} \cdot \vec{p} - K^2. \quad (33)$$

After introducing this approximate relation, the Dirac equation for the upper component (28) becomes

$$[-i\vec{K} \cdot \vec{\nabla} - K^2 + M(V_c + V_{so}[\vec{\sigma} \cdot (\vec{r} \times \vec{K}) - i\vec{r} \cdot \vec{K}])]u_{\vec{k},s}^{(+)} = 0, \quad (34)$$

where the momentum operators in the spin orbit and Darwin terms are substituted by \vec{K} . Remark that the above equation is now linear in the momentum operator. In the eikonal limit, the scattering wave functions take on the form

$$u_{\vec{k},s}^{(+)} = e^{i\vec{k} \cdot \vec{r}} e^{iS(\vec{r})} \chi_{\frac{1}{2}m_s}. \quad (35)$$

Inserting this into Eq. (34), yields an expression for the eikonal phase [21]. Defining the z -axis along the direction of the average momentum \vec{K} , this phase can be written in an integral form as :

$$iS(\vec{b}, z) = -i\frac{M}{K} \int_{-\infty}^z dz' [V_c(\vec{b}, z') + V_{so}(\vec{b}, z')[\vec{\sigma} \cdot (\vec{b} \times \vec{K}) - iKz']], \quad (36)$$

where we have introduced the notation $\vec{r} \equiv (\vec{b}, z)$. The scattering wave function, which is proportional to

$$\phi_{\vec{k},s}^{(+)} \sim \left[\frac{1}{E+M+V_s-V_v} \vec{\sigma} \cdot \vec{p} \right] e^{i\vec{k} \cdot \vec{r}} e^{iS(\vec{r})} \chi_{\frac{1}{2}m_s}, \quad (37)$$

is normalized such that

$$\overline{\phi_{\vec{k},s}^{(+)}} \phi_{\vec{k},s}^{(+)} = 1. \quad (38)$$

This wave function differs from the plane-wave solution in two respects. First, the lower component exhibits the dynamical enhancement due to the combination of the scalar and vector potentials. Second, the eikonal phase $e^{iS(\vec{r})}$ accounts for the interactions that the struck nucleon undergoes in its way out of the nucleus. The calculation of the eikonal phase (36) involves a transformation to a reference frame other than the usual laboratory or center-of-mass frame, namely the frame where the average momentum is pointing along the z -axis. As the eikonal phase has to be re-evaluated for every (\vec{b}, z) point in space, the Dirac eikonal ($e, e'p$) calculations are very demanding as far as computing power is concerned. In evaluating the matrix elements, the radial integrations were performed on a 0.1 fm mesh. It is worth remarking that the standard Glauber approach followed in many studies involves an extra approximation apart from the ones discussed above. Indeed, in evaluating the eikonal phase from Eq. (36) one frequently approximates the z -dependence of the potentials by a delta function.

D. Off-shell electron-proton coupling

We express the matrix elements of the nucleon current in the usual form

$$\langle P_f S_f | J^\mu | P_i S_i \rangle = \bar{u}_f \Gamma^\mu(P_f, P_i) u_i, \quad (39)$$

where Γ^μ is the electromagnetic vertex function for the nucleon and u_i (u_f) the nucleon spinors. As discussed in many works [24–28], some arbitrariness, often referred to as the “off-shell ambiguity”, surrounds the choice for the functional form of the vertex function Γ^μ . For a free nucleon, Γ^μ can be expressed in several fully equivalent forms

$$\Gamma_{cc1}^\mu = G_M(Q^2) \gamma^\mu - \frac{\kappa}{2M} F_2(Q^2) (P_i^\mu + P_f^\mu), \quad (40)$$

$$\Gamma_{cc2}^\mu = F_1(Q^2) \gamma^\mu + i \frac{\kappa}{2M} F_2(Q^2) \sigma^{\mu\nu} q_\nu, \quad (41)$$

$$\Gamma_{cc3}^\mu = \frac{1}{2M} F_1(Q^2) (P_i^\mu + P_f^\mu) + i \frac{1}{2M} G_M(Q^2) \sigma^{\mu\nu} q_\nu, \quad (42)$$

where F_1 is the Dirac, F_2 the Pauli form factor and κ is the anomalous magnetic moment. The relation with the Sachs electric and magnetic form factors is established through $G_E = F_1 - \tau \kappa F_2$ and $G_M = F_1 + \kappa F_2$, with $\tau \equiv Q^2/4m^2$.

When considering bound (or, “off-shell”) nucleons, however, the above vertex functions can no longer be guaranteed to produce the same results. As a matter of fact, explicit current conservation is rather an exception than a rule in most calculations that deal with ($e, e'p$) reactions from finite nuclei. In nuclear physics, the most widely used procedure to “effectively” restore current conservation is based on modifying the longitudinal component of the nuclear vector current using the substitution

$$J_z \rightarrow \frac{\omega}{q} J_0. \quad (43)$$

This procedure is partly inspired on the observation that meson-exchange and isobar terms enter the charge current operator in a higher relativistic order than they used to do for the vector current. There exist several other prescriptions which are meant to restore current conservation. Along similar lines, the charge operator can be replaced by

$$J_0 \rightarrow \frac{q}{\omega} J_z. \quad (44)$$

One can also construct a vertex function that guarantees current conservation for any initial and final nucleon state. This can be achieved for example by adding an extra term to the vertex [29]

$$\Gamma_{DON}^\mu = F_1(Q^2) \gamma^\mu + i \frac{\kappa}{2M} F_2(Q^2) \sigma^{\mu\nu} q_\nu + F_1(Q^2) \frac{\not{q} q^\mu}{Q^2}, \quad (45)$$

which is also equivalent to the Eqs. (40-42) in the free nucleon case. An operator derived from the generalized Ward-Takahashi identity reads [26]

$$\Gamma_{WT}^\mu = \gamma^\mu - i \frac{\kappa}{2M} F_2(Q^2) \sigma^{\mu\nu} q_\nu + [F_1(Q^2) - 1] \frac{\not{q} q^\mu + Q^2 \gamma^\mu}{Q^2}. \quad (46)$$

III. RESULTS

A. Final state interactions and the eikonal approximation

We start our ($e, e'p$) investigations within the relativistic eikonal approximation for the kinematics of an $^{16}\text{O}(e, e'p)$ experiment that was recently performed at Jefferson Lab [12]. In this experiment, the separated $^{16}\text{O}(e, e'p)$ structure functions are measured at $Q^2 = 0.8$ (GeV/c) 2 and $\omega = 0.439$ GeV for missing (or, initial) proton momenta $p_m = |\vec{k}_f - \vec{q}|$ below 355 MeV/c. The variation in missing momentum was achieved by varying the detection angle of the ejected proton with respect to the direction of the momentum transfer (“quasi-perpendicular kinematics”). The measured cross sections for knockout from the $1p_{1/2}$ and $1p_{3/2}$ levels are depicted in Fig. 3 along with the predictions of our relativistic eikonal calculations. A spectroscopic factor of 0.6 was adopted for all bound levels, and the standard dipole form was used for the electromagnetic form factors. At low missing momenta, the eikonal results shown in Fig.

3 produce a fair description of the data. As a comparison, the results of a relativistic plane wave calculation in the impulse approximation (RPWIA) are also displayed. Through comparing the plane-wave and the eikonal calculations, thereby keeping all other ingredients of the calculations identical, one can evaluate how the eikonal method deals with final state interactions (FSI). In the eikonal calculations, the dips of the RPWIA calculations are filled in, and, at low missing momenta the RPWIA cross sections are reduced. These two features reflect nothing but the usual impact of the final-state interactions on the $A(e, e'p)$ angular cross sections. The limitations of the eikonal approximation ($q \gg k_i$) are immediately visible at higher missing momenta ($p_m \geq 250$ MeV/c). Here, the eikonal cross sections largely overshoot both the RPWIA results and the data and should by no means be considered as realistic. It is worth remarking that the data closely follow the trend set by the RPWIA curves. As a matter of fact, whereas the eikonal calculations predict huge effects from final-state interactions at large transverse missing momenta, the data seem to suggest rather the opposite effect. We consider this observation as one of the major findings of this work.

One may wonder whether the observed behaviour of the eikonal results at higher missing momenta in Fig. 3 is a mere consequence of the small-angle approximation contained in Eq. (33), or whether the adopted model assumptions for computing the scattering states is also (partly) at the origin of this pathological behavior. To address this question, we have performed calculations for various fixed recoil angles θ defined as

$$\cos \theta = \frac{\vec{p}_m \cdot \vec{q}}{|\vec{p}_m| |\vec{q}|}. \quad (47)$$

The results are displayed in terms of the reduced cross section ρ which is defined in the standard fashion as the differential cross section, divided by a kinematical factor times the “*CC1*” off-shell electron-nucleon cross section of Ref. [30]. For the results of Figure 4 we considered in-plane kinematics at a fixed value of the outgoing proton momentum ($k_f=1$ (GeV)/c) and an initial electron energy of 2.4 GeV. The variation in missing momentum is achieved by changing the q . For recoil angles $\theta = 0^\circ$ (“parallel kinematics”) the eikonal calculations do not exhibit an unrealistic behavior up to $p_m=0.5$ GeV/c, which is the highest missing momentum considered here. With increasing recoil angles, and consequently, growing “transverse” components in the missing momenta the “unrealistic” behaviour of the eikonal results becomes manifest. Accordingly, the accuracy of the eikonal method based on the small-angle approximation of Eq. (33) can only be guaranteed for proton knockout in a small cone about the momentum transfer. A similar quantitative behaviour as a function of the recoil angle to what is observed in Fig. 4 was reported in Ref. [3] for $d(e, e'p)n$ cross sections determined in a Glauber framework. We conclude this section with remarking that the eikonal method does not exclude situations with high initial (or, missing) momenta, it only requires that the perpendicular component of ejectiles’s momentum \vec{k}_f is sufficiently small. It speaks for itself that such conditions are best fulfilled as one approaches parallel kinematics. This observation puts serious constraints on the applicability of the Glauber method, that is based on the eikonal approximation, for modelling the final-state interactions in high-energy ($e, e'p$) reactions from nuclei. However, it should be noted that our framework does use purely real scalar and vector potentials. More realistic scattering potentials demand an imaginary part that accounts for the inelastic channels that are open during the reaction process. The Glauber approach effectively includes these inelastic channels and on these grounds one may expect that its range of applicability is somewhat wider than what is observed here. With the eye on defining the region of validity for the eikonal approximation more clearly, we have studied differential cross sections for various Q^2 . In Fig. 5, we display the computed differential cross sections for the $^{12}\text{C}(e, e'p)^{11}\text{B}(1p_{3/2}^{-1})$ process against the missing momentum for Q^2 varying between 1 and 20 (GeV/c) 2 . Hereby, quasi-elastic conditions were imposed. The arrow indicates the missing momentum where the slope of the eikonal differential cross section starts deviating from the trend set by the RPWIA cross section. In the light of the conclusions drawn from the comparison between data and the eikonal curves in Fig. 3, the eikonal results should be regarded with care beyond this missing momentum. Furthermore, it is clear that the change in the slope of the angular cross section becomes more and more pronounced as Q^2 increases. It is apparent from Fig. 5 that the eikonal differential cross section changes slope at about $p_m=250$ MeV/c for all values of Q^2 considered. We remark that we imposed quasi-elastic conditions for all cases contained in Fig. 5. As a consequence, the momentum of the ejected nucleon varies quite dramatically as one moves up in Q^2 . The uniform behaviour of all curves contained in Fig. 5 allows one to write down a relation between the transferred momentum \vec{q} and the polar scattering angle θ : $|\vec{q}| \theta \leq 250$ MeV rad. This simple relation could serve as a conservative guideline to determine the opening angle of the cone in which the outgoing proton momentum has to reside to ascertain that the eikonal approximation produces “realistic” results. This limitation of the eikonal method can also be inferred from the results contained in Refs. [9,31]. Indeed, in Figs. 3 and 4 of Ref. [9] one can confirm that the above relation between $|\vec{q}|$ and θ defines the missing momentum at which a sudden change in the p_m dependence of the calculated cross sections is observed. The above relation can be understood as follows. In quasi-perpendicular and quasi-elastic kinematics, the missing momentum roughly equals the transverse momentum of the ejected nucleon. With increasing momentum transfer, the longitudinal momentum of the escaping nucleon increases correspondingly while its transverse momentum has to stay smaller than the suggested value of 250 MeV/c. Hence, the sine of the

angle between the transferred momentum and the ejectile's momentum has to decrease. Since we are dealing with small angles, $\sin(\theta)$ can be approximated by θ . The opening angle of the cone in which the eikonal approximation is valid, can be inferred to be independent of Q^2 in the Lorentz frame where the ejected nucleon is at rest. When transforming back to the labframe, lateral dimensions become dilated, and, thus, angles contracted.

B. The Q^2 evolution of off-shell effects

A major point of concern in any $A(e, e'p)B$ calculation are the ambiguities regarding the off-shell electron-proton coupling. Most calculations do not obey current conservation and a variety of prescriptions have been proposed to partially cure this deficiency. Here we adopt a heuristic view and estimate the sensitivity of the calculated observables by comparing the results obtained with different viable prescriptions for the electron-proton coupling. Amongst the infinite number of possible prescriptions for the off-shell electron-proton coupling we have selected four that are frequently used in literature. Figure 6 shows the separated structure functions for $1p_{1/2}$ knockout in the kinematics of Fig. 3. Current conservation was imposed by either modifying the longitudinal component of the vector current operator (hereafter denoted as the “J0 method”), or by modifying the charge operator (hereafter denoted as the “J3 method”), along the lines of Eqs. (43) and (44). Note that for the operator of Eq. (45), both methods yield the same results, since, by construction, this operator is current conserving, regardless of the method adopted to compute the wave function for the initial and final state.

Turning to the results shown in Fig. 6, the predicted strengths in the longitudinal structure functions R_L and R_{TL} depend heavily on the choice made for the electron-proton coupling. For the $CC1$ prescription, for example, the values obtained with the J3 method are several times bigger than those obtained within the J0 method. The predicted differences among the various current operators within one scheme (“J0” or “J3”) are also sizeable. The ambiguities are, however, much smaller for the calculations performed with the $J_z \rightarrow \frac{\omega}{q}J_0$ substitution. This clearly speaks in favor of this recipe which is mostly used in $A(e, e'p)$ calculations. The R_{TT} and R_T structure functions are, obviously, insensitive to whether the “J0” or “J3” method is adopted. All adopted electron-proton couplings but the $CC1$ one produce the same results in the R_T and R_{TT} responses.

With increasing Q^2 and the corresponding decreasing distance scale, the role of off-shell ambiguities in the photon-nucleus coupling is expected to decline and the impulse approximation is believed to become increasingly accurate. In order to investigate the degree and rate to which this virtue may be realized, we have performed calculations for kinematics in the range of $0.8 \leq Q^2 \leq 20$ (GeV/c)². We use two techniques to estimate the relative importance of the off-shell effects as a function of Q^2 . First, results computed with the “J0” and “J3” method can be compared. Second, predictions with various choices for the electron-proton coupling are confronted with one another. The validity of the IA is then established whenever the final result happens to become independent of the adopted choice. In order to assess the degree to which this independence is realized, we have considered ratios of structure functions for some fixed kinematics but calculated with different choices for the electron-proton coupling. As a benchmark calculation, we have computed $^{12}\text{C}(e, e'p)^{11}\text{B}(1p_{3/2}^{-1})$ observables in quasi-elastic kinematics for several values of the four-momentum transfer. The results are shown in Figs. 7 and 8. Fig. 7 shows for several observables the ratio of the values obtained with the “J3” scheme to the corresponding prediction using the “J0” scheme. Fig. 8 shows the ratio of the strengths obtained with the $CC1$ vertex function compared to the corresponding predictions with the $CC2$ form. Remark that in the limit of vanishing off-shell effects, these ratios should equal one. It is indeed found that the calculations that are based on the substitution $J_z \rightarrow \frac{\omega}{q}J_0$, tend to converge to those based on $J_0 \rightarrow \frac{q}{\omega}J_z$ with increasing energy transfer. This is particularly the case at low missing momenta, where the decrease in the longitudinal response is almost exponential. The overall behaviour is identical for the higher missing momentum case ($p_m = 150$ MeV/c), but the rate of decrease is somewhat slower. This can be attributed to the fact that at higher momenta, hence, greater angles, the transverse components of the vertex functions play a more important role. Looking at Fig. 8 one can essentially draw the same conclusions. The predictions with the different prescriptions also converge to each other as the energy is increased. Again this convergence is more pronounced for the low missing momentum case. This feature is most apparent in the purely transverse channel, which dominates the cross section at sufficiently high energies. It appears thus as if off-shell ambiguities, speaking in terms of strengths and absolute cross sections, are of far less concern at higher Q^2 than they used to be in the $Q^2 \leq 1$ (GeV/c)² region, where most of the data have been accumulated up to now. The interference structure functions R_{TT} and R_{TL} are subject to off-shell ambiguities that are apparently extending to the highest four-momentum transfers considered here. This feature was already established in Ref. [29] and explained by referring to the large weight of the negative energy solutions in the interference structure functions R_{TL} and R_{TT} .

C. Relativistic Effects

Recently, there have been several claims for strong indications for genuine (or, “dynamic”) relativistic effects in $A(\vec{e}, e'\vec{p})$ observables [12,32–34]. In an attempt to implement some of these effects in calculations based on a Schrödinger picture, several techniques to obtain a “relativized version” of the electron-nucleus vertex have been developed. In leading order in a p/M expansion these “relativized” electron-nucleus vertices typically miss the coupling between the lower components in the bound and scattering states. For that reason, we interpret the effect of the coupling between the lower components in the bound and scattering states as a measure for the importance of relativistic effects. In Fig. 9 we display results of fully relativistic $^{12}\text{C}(e, e'p)^{11}\text{B}(1p_{3/2}^{-1})$ calculations and calculations in which the specific coupling between the lower components in the bound and scattering states have been left out. We consider quasi-elastic conditions and study the Q^2 evolution of the structure functions for two values of the missing momentum ($p_m = 0$ and 150 MeV/c) both corresponding with small recoil angles. Hence, the results of Fig. 9 refer to kinematic conditions for which the eikonal approximation is justified. A rather complex and oscillatory Q^2 dependence of the relativistic effects emerges from our numerical calculations. Looking first at the $p_m \approx 0$ MeV/c case, which nearly corresponds with parallel kinematics, we observe that for both the longitudinal and transverse structure functions, the impact of the coupling amongst the lower components first increases, and then tends to become fairly constant for higher values of ω . The genuine relativistic effect stemming from the coupling between the lower components in the initial and final states is larger in the longitudinal than in the transverse channel. It is noteworthy that in the cross section the impact of the “relativistic dynamical effects” never exceeds the 10 % level. If we turn our attention to the interference structure functions R_{TL} and R_{TT} , the relativistic effects grow in importance. Especially for the R_{TL} structure function the effects are large and extend to the smallest values of Q^2 considered here. This enhanced sensitivity of the R_{TL} response to relativistic effects, even when relatively low values of Q^2 are probed, complies with the conclusions drawn in other studies [28,32,35–37]. Also the tendency of the relativistic effects to increase the cross section when higher values of p_m are probed complies with the findings of earlier studies [38]. A quantity that is relatively easy to access experimentally and depends heavily upon the R_{TL} term, is the so-called left-right asymmetry A_{LT}

$$A_{LT} = \frac{\sigma(\phi = 0^\circ) - \sigma(\phi = 180^\circ)}{\sigma(\phi = 0^\circ) + \sigma(\phi = 180^\circ)} = \frac{v_{TL}R_{TL}}{v_LR_L + v_TR_T + v_{TT}R_{TT}}. \quad (48)$$

In Fig. 10 we have plotted the left-right asymmetry for both $1p_{1/2}$ and $1p_{3/2}$ knockout from ^{16}O in the kinematics of Fig. 3. It is indeed verified that the asymmetry is very sensitive to relativistic effects. As has been reported, relativistic effects enhance the asymmetry further, and this enhancement is more pronounced for the $1p_{1/2}$ knockout reaction. The role played by the lower components in this dynamical enhancement of the left-right asymmetry can be further clarified by looking at the results of Fig. 11. In this figure, we plot the left-right asymmetry for $1p_{3/2}$ knockout from ^{12}C , for different Q^2 and quasi-elastic conditions. Looking at the fully relativistic curves, we observe a gradual decrease of the asymmetry with increasing Q^2 . At the same time, the relative contribution of the “non-relativistic” contribution to A_{LT} diminishes. This feature indicates that the asymmetry A_{LT} is nearly exclusively generated by the coupling between the lower components as Q^2 increases.

IV. SUMMARY

We have outlined a fully relativistic eikonal framework for calculating cross sections for $(e, e'p)$ reactions from spherical nuclei at intermediate and high four-momentum transfers and carried out $^{12}\text{C}(e, e'p)$ and $^{16}\text{O}(e, e'p)$ calculations for a variety of kinematical conditions, thereby covering four-momentum transfers in the range $0.8 \leq Q^2 \leq 20$ (GeV/c)². Our results illustrate that the validity of the eikonal method is confined to proton emission in a cone with a relatively small opening angle about the direction of the virtual photon’s momentum. This observation puts serious constraints on the applicability of the Glauber method, that is based on the eikonal approximation, for modelling the final-state interactions in high-energy $(e, e'p)$ reactions from nuclei. Incorporation of the inelastic channels in the eikonal method is however needed to fully appreciate the limits of the Glauber model, and work along these lines is in progress. In line with the expectations, our investigations illustrate that the uncertainties induced by off-shell ambiguities on the calculated observables diminish as Q^2 increases. Nevertheless, in the relativistic eikonal framework four-momentum transfers of the order 5 (GeV/c)² appear necessary to assure that the effect of the off-shell ambiguities can be brought down to the percent level. Our theoretical framework permits to assess the impact of the relativistic effects over a wide energy range. The impact of the lower components on the $(e, e'p)$ observables is observed to be significant over the whole Q^2 range studied. Especially the left-right asymmetry lends itself very well to study these effects of genuine relativistic origin.

Acknowledgement

This work was supported by the Fund for Scientific Research of Flanders under contract No. 4.0061.99 and the University Research Council.

-
- [1] Vijay R. Pandharipande, Ingo Sick, and Peter K. A. deWitt Huberts, *Rev. Mod. Phys.* **69** (1997) 981.
- [2] L.L. Frankfurt, G.A. Miller and M.I. Strikman, *Comments Nucl. Part. Phys.* **21** (1992) 1.
- [3] S. Jeschonnek and T.W. Donnelly, *Phys. Rev. C* **59** (1999) 2676.
- [4] G.D. Alkharov, S.L. Belostotsky and A.A. Voroboyov, *Phys. Repts.* **42** (1978) 89.
- [5] L.L. Frankfurt, E.J. Moniz, M.M. Sargsyan and M.I. Strikman, *Phys. Rev. C* **51** (1995), 3435.
- [6] O. Benhar, S. Fantoni, N.N. Nikolaev, J. Speth, A.A. Usmani and B.G. Zakharov, *Z. Phys. A* **355** (1996) 267.
- [7] N.N. Nikolaev, A. Szczurek, J. Speth, J. Wambach, B.G. Zakharov and V.R. Zoller, *Nucl. Phys.* **A582** (1995) 665.
- [8] C. Ciofi degli Atti and D. Treleani, *Phys. Rev. C* **60** (1999) 024602.
- [9] A. Bianconi and M. Radici, *Phys. Lett.* **B363** (1995) 24.
- [10] A.S. Rinat and M.F. Taragin, *Nucl. Phys.* **A623** (1997) 519.
- [11] Akihisa Kohama, Koichi Yazaki and Ryoichi Seki, *Nucl. Phys.* **A662** (2000) 175.
- [12] J. Gao *et al.*, *Phys. Rev. Lett.* **84** (2000) 3265.
- [13] A.S. Raskin and T.W. Donnelly, *Ann. Phys.* **191** (1989) 78.
- [14] J.D. Bjorken and S.D. Drell, *Relativistic Quantum Mechanics* (McGraw-Hill, New York, 1964).
- [15] B.D. Serot and J.D. Walecka, *Adv. Nucl. Phys.* **16** (1986) 1.
- [16] C.J. Horowitz and B.D. Serot, *Nucl. Phys.* **A368** (1981) 503.
- [17] J.M. Udias *et al.*, *Phys. Rev. C* **8** (1993) 2731.
- [18] Y. Yin, D.S. Onley and L.E. Wright, *Phys. Rev. C* **45** (1992) 1311.
- [19] J.I. Johansson, H.S. Sherif and G.M. Lotz, *Nucl. Phys.* **A605** (1996) 517.
- [20] E.D. Cooper, S. Hama, B.C. Clark and R.L. Mercer, *Phys. Rev. C* **47** (1993) 297.
- [21] H. Ito, S.E. Koonin and R. Seki, *Phys. Rev. C* **56** (1997) 3231.
- [22] O. Benhar, N.N. Nikolaev, J. Speth, A.A. Usmani and B.G. Zakharov, nucl-th/0001035 and *Nucl. Phys. A* (in press)
- [23] R.D. Amado, J. Piekarewicz, D.A. Sparrow and J.A. McNeil, *Phys. Rev. C* **28** (1983) 1663.
- [24] S. Pollock, H.W.L. Naus and J.H. Koch, *Phys. Rev. C* **53** (1996) 2304.
- [25] S.I. Nagorny and A.E.L. Dieperink, *Eur. Phys. J.* **A5** (1999) 417.
- [26] F. Gross and D.O. Riska, *Phys. Rev. C* **36** (1987) 1928.
- [27] J.J. Kelly, *Phys. Rev. C* **56** (1997) 2672.
- [28] J.J. Kelly, *Phys. Rev. C* **60** (1999) 044609.
- [29] J.A. Caballero, T.W. Donnelly, E. Moya de Guerra and J.M. Udias, *Nucl. Phys.* **A632** (1998) 323.
- [30] T. De Forest, *Nucl. Phys.* **A392** (1983) 232.
- [31] A. Bianconi and M. Radici, *Phys. Rev. C* **54** (1996) 3117.
- [32] S. Gardner and J. Piekarewicz, *Phys. Rev. C* **50** (1994) 2822.
- [33] J.M. Udias, J.A. Caballero, E. Moya de Guerra, J.E. Amaro and T.W. Donnelly, *Phys. Rev. Lett.* **83** (1999) 5451.
- [34] J.I. Johansson and H.S. Sherif, *Phys. Rev. C* **59** (1999) 3481.
- [35] J. Ryckebusch, D. Debruyne, W. Van Nespén and S. Janssen, *Phys. Rev. C* **60** (1999) 034604.
- [36] S. Ulrych and H. Müther, *Nucl. Phys.* **A641** (1998) 499.
- [37] S. Gilad, W. Bertozzi and Z.-L. Zhou, *Nucl. Phys.* **A631** (1998) 276c.
- [38] J.M. Udias, P. Sarriguren, E. Moya de Guerra, J.A. Caballero, *Phys. Rev. C* **53** (1996) 1488.

FIG. 1. The calculated scalar (ρ_s), baryon (ρ_B), rho (ρ_3) and proton (ρ_P) density distributions in ^{12}C and ^{16}O .

FIG. 2. The radial dependence of the scalar and vector potentials (in absolute values) as obtained from relativistic Hartree calculations for ^{12}C and ^{16}O .

FIG. 3. Measured $^{16}\text{O}(e, e'p)$ cross sections compared to relativistic eikonal and RPWIA calculations at $\epsilon = 2.4$ GeV, $q = 1$ GeV/c and $\omega = 0.439$ GeV in quasi-perpendicular kinematics. The calculations use the current operator *CC1*. The data are from Ref. [12].

FIG. 4. The reduced cross section for the $^{16}\text{O}(e, e'p)^{15}\text{N}(1p_{3/2}^{-1})$ reaction versus missing momentum at three values of the recoil angle θ . A fixed outgoing proton momentum of $|\vec{p}| = 1$ GeV was considered. The solid line shows the fully relativistic eikonal calculation, while the dashed one shows the RPWIA results. The calculations use the *CC1* prescription.

FIG. 5. The differential cross section for the $^{12}\text{C}(e, e'p)^{11}\text{B}(1p_{3/2}^{-1})$ reaction versus missing momentum at six different values for Q^2 . Quasi-elastic conditions and perpendicular kinematics were considered.

FIG. 6. The different structure functions versus missing momentum for $1p_{1/2}$ knockout from ^{16}O in the kinematics of Fig. 3. The calculations in the left column imposed current conservation by replacing the longitudinal component of the vector current operator (Eq. 43), while for the results in the right column the charge density operator was modified according to Eq. (44). The curves refer to the different off-shell prescriptions as they were introduced in Sect. IID.

FIG. 7. The Q^2 dependence of the sensitivity of the calculated $(e, e'p)$ structure functions to the choice for the electron-nucleus vertex for $1p_{3/2}$ knockout from ^{12}C in quasi-elastic kinematics. The curves show for the various observables the ratio of the predictions with the “J3” method to those obtained with the “J0” method. Solid (dashed) line corresponds with the $p_m = 0$ MeV/c ($p_m = 150$ MeV/c) situation.

FIG. 8. The Q^2 dependence of the sensitivity of the $(e, e'p)$ structure functions to the choice for the electron-nucleus vertex for $1p_{3/2}$ knockout from ^{12}C . The curves display the ratio of the predictions using the vertex function Γ_{cc1}^μ to those using Γ_{cc2}^μ . Solid (dashed) lines correspond with $p_m = 0$ MeV/c ($p_m = 150$ MeV/c).

FIG. 9. The Q^2 dependence of the sensitivity of the $(e, e'p)$ structure functions to dynamical relativistic effects. The curves show for $1p_{3/2}$ knockout from ^{12}C the ratio of the fully relativistic results to the predictions when the coupling between the lower components is neglected. The solid (dashed) line presents results for the situation $p_m = 0$ MeV/c ($p_m = 150$ MeV/c).

FIG. 10. The left-right asymmetry A_{LT} for both $1p_{1/2}$ and $1p_{3/2}$ knockout from ^{16}O in the kinematics of Fig. 3. The data are from Ref. [12].

FIG. 11. The left-right asymmetry A_{LT} for $1p_{3/2}$ knockout from ^{12}C for different Q^2 , under quasi-elastic conditions and perpendicular kinematics.

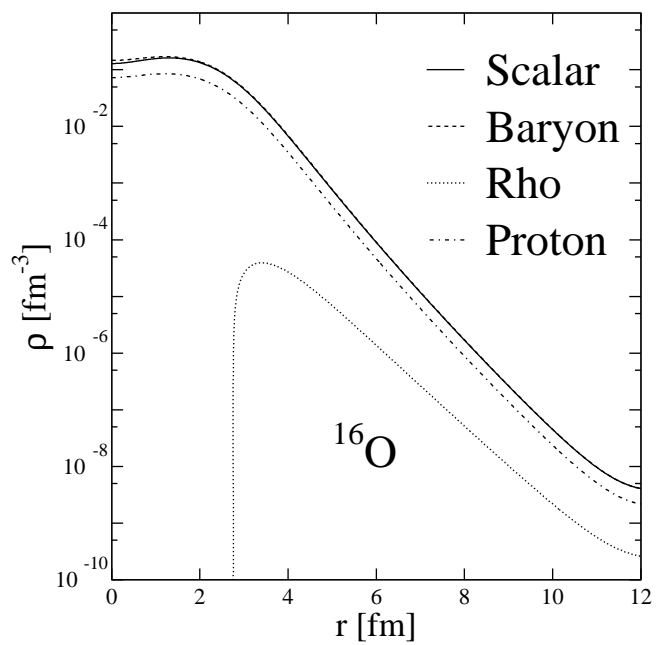
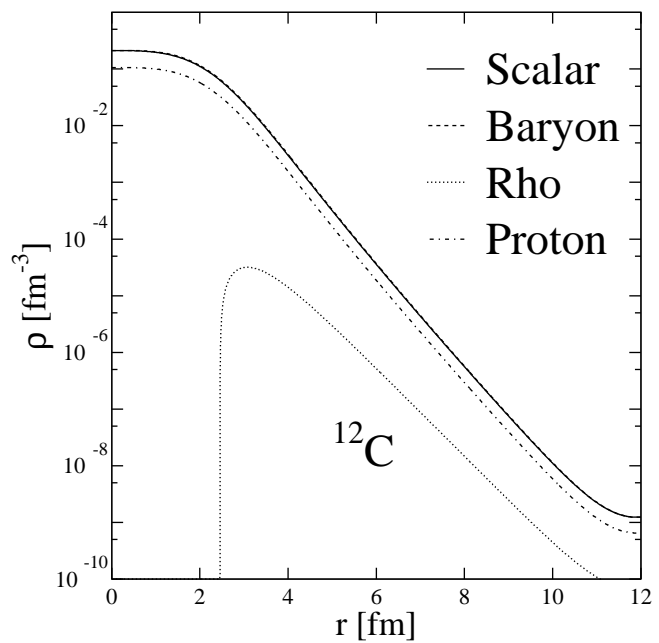


Figure 1

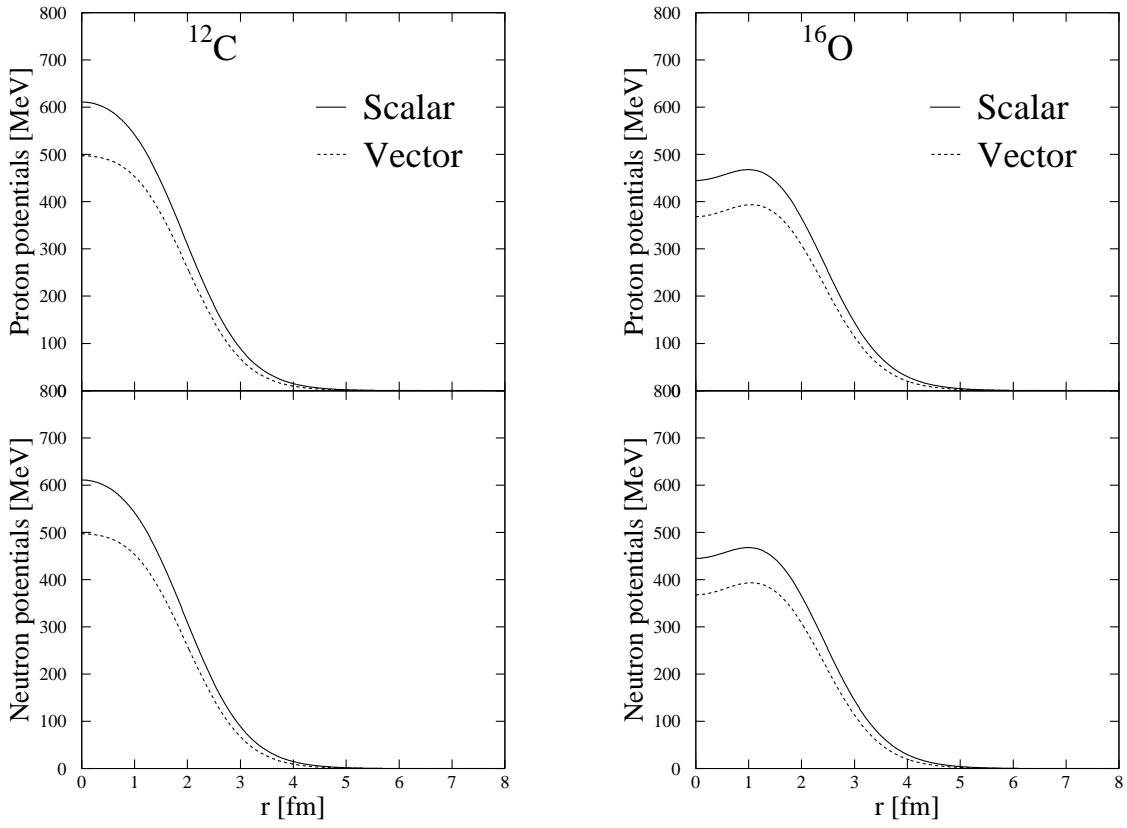


Figure 2

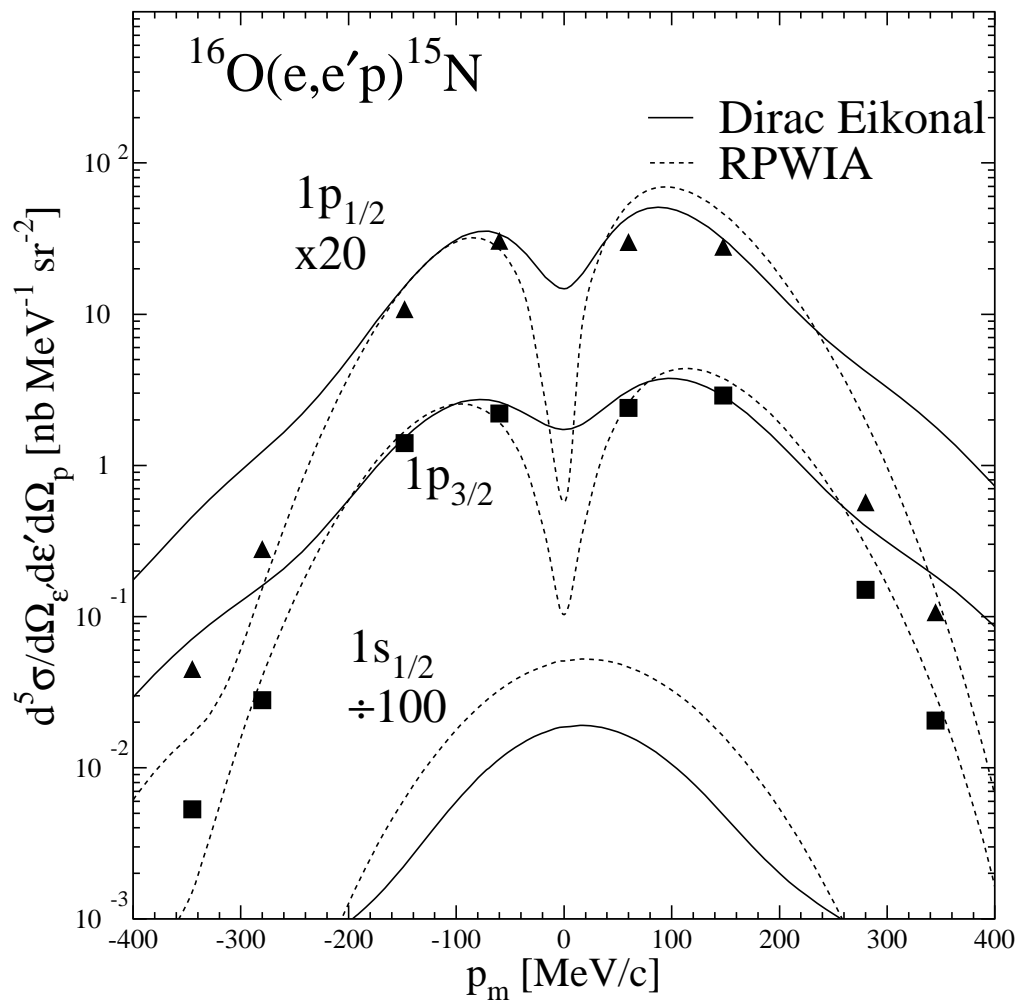


Figure 3

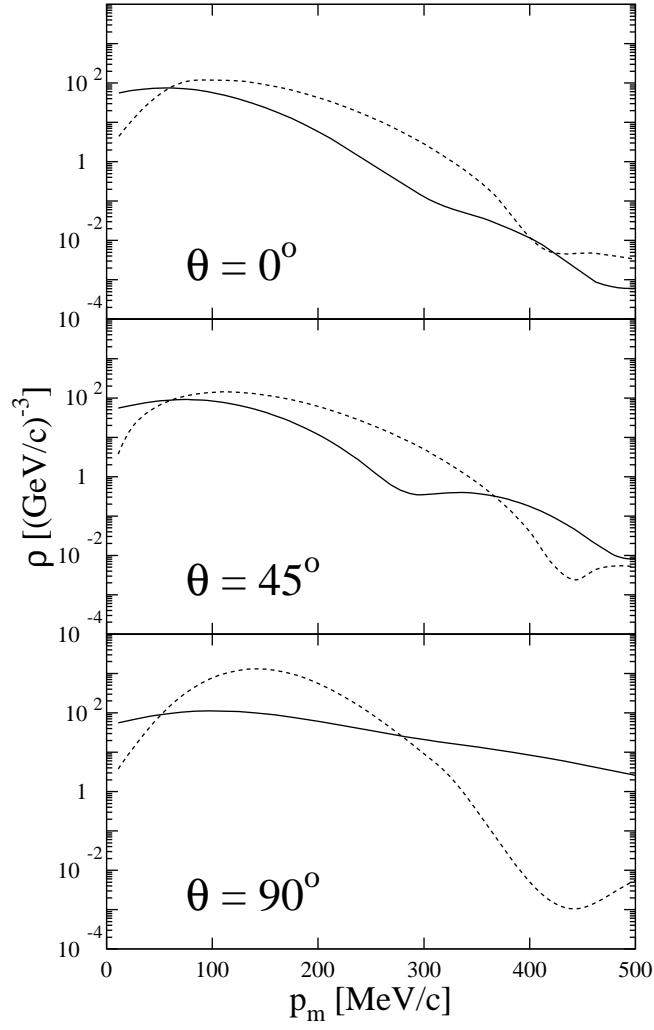


Figure 4

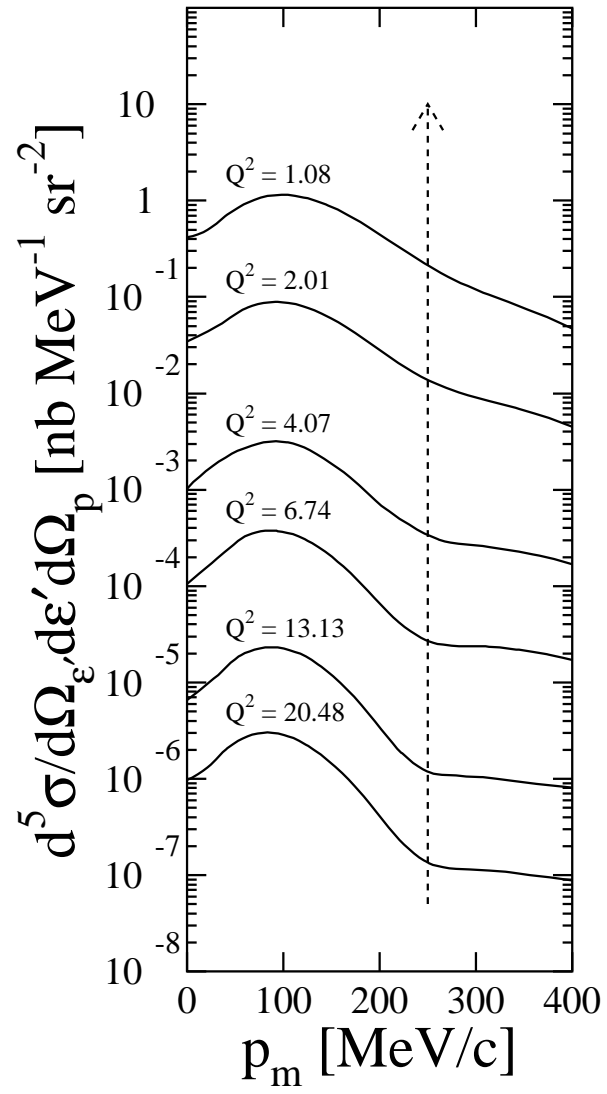


Figure 5

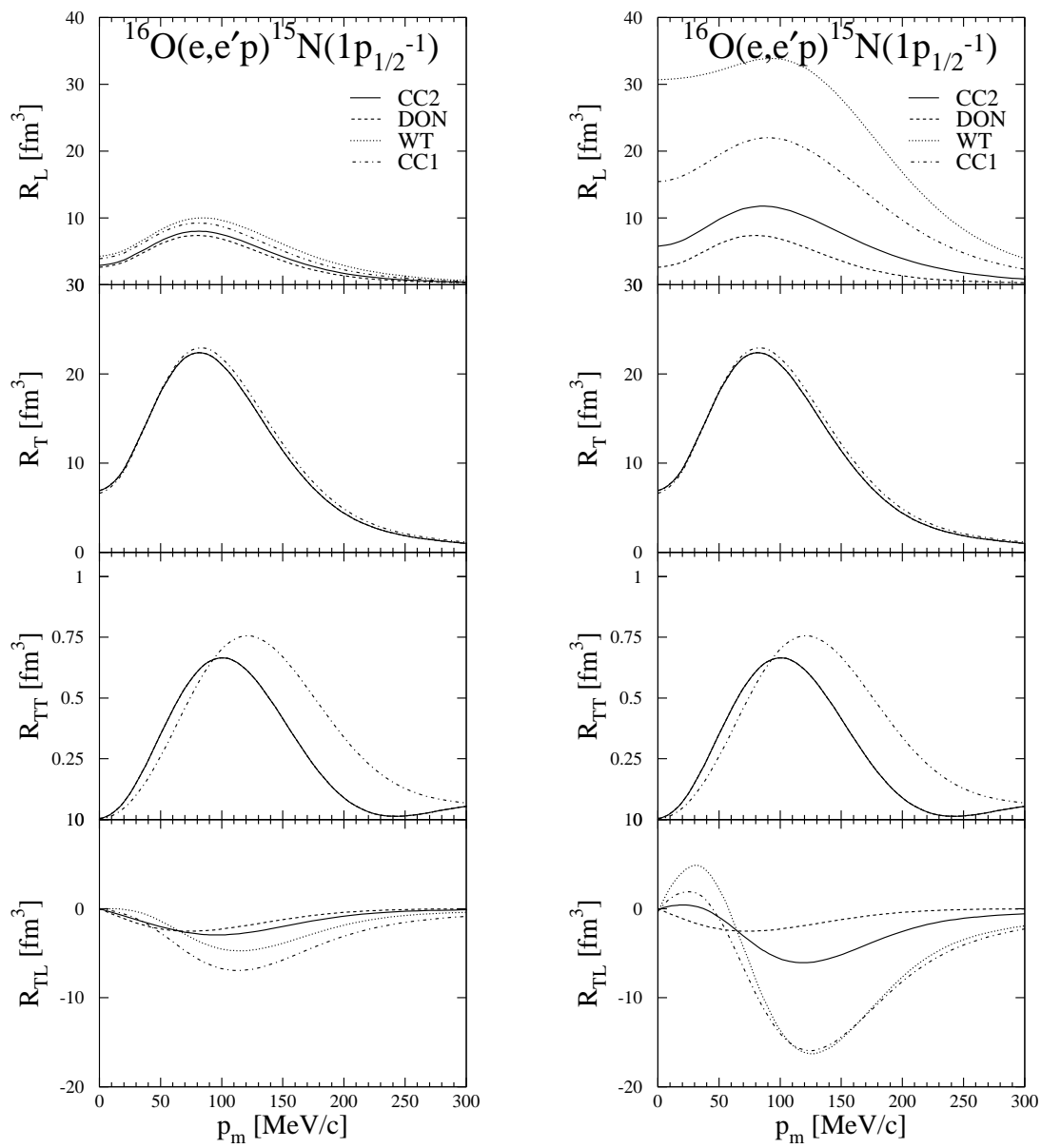


Figure 6

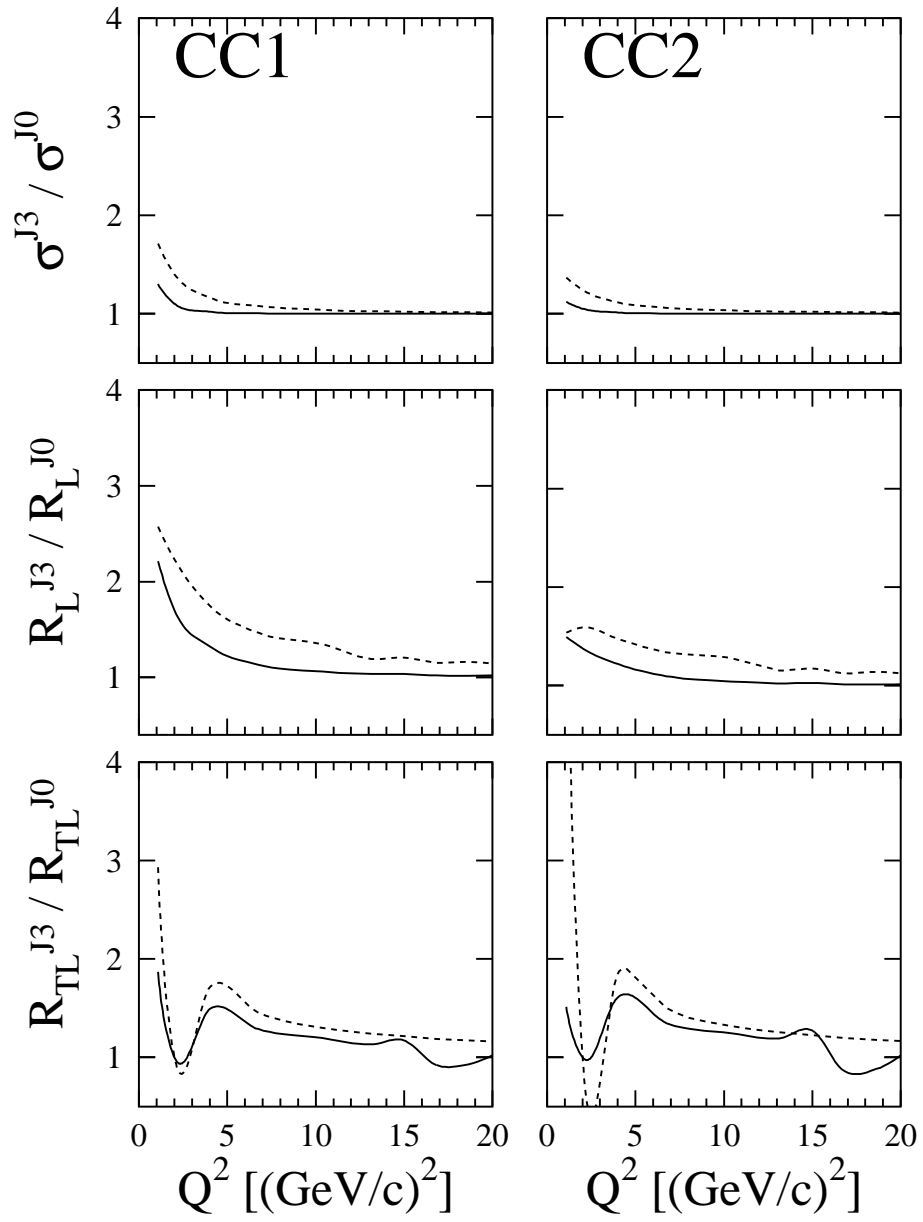


Figure 7

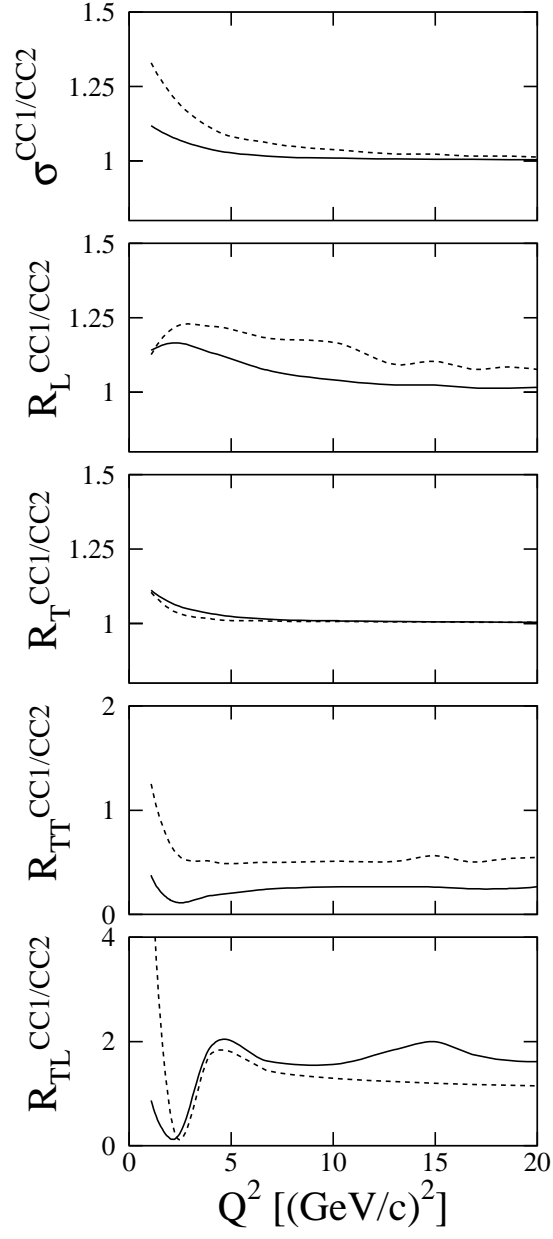


Figure 8

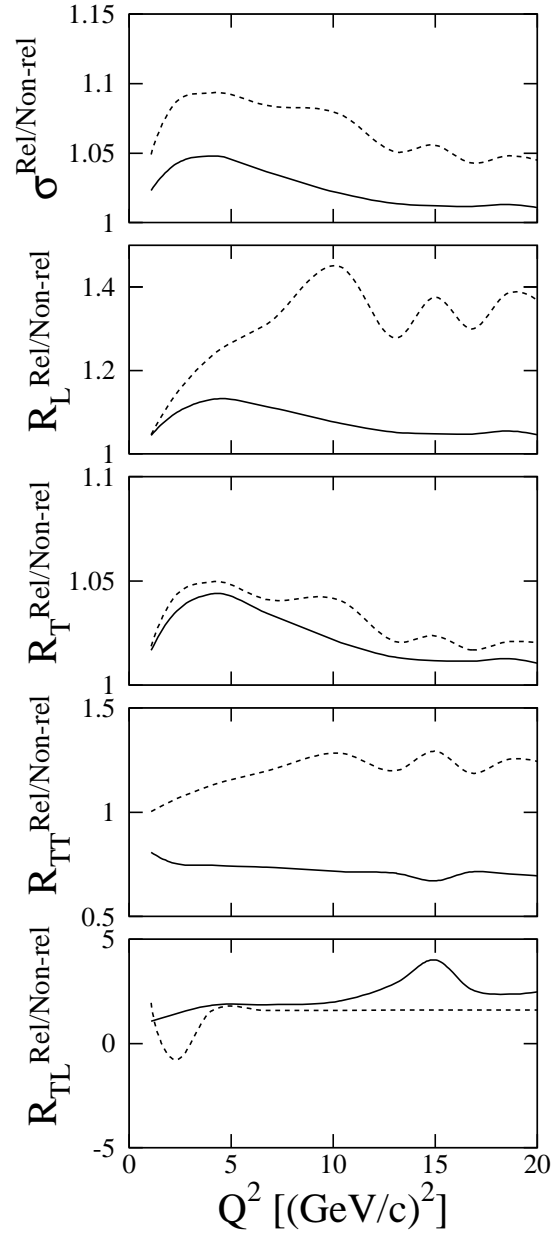


Figure 9

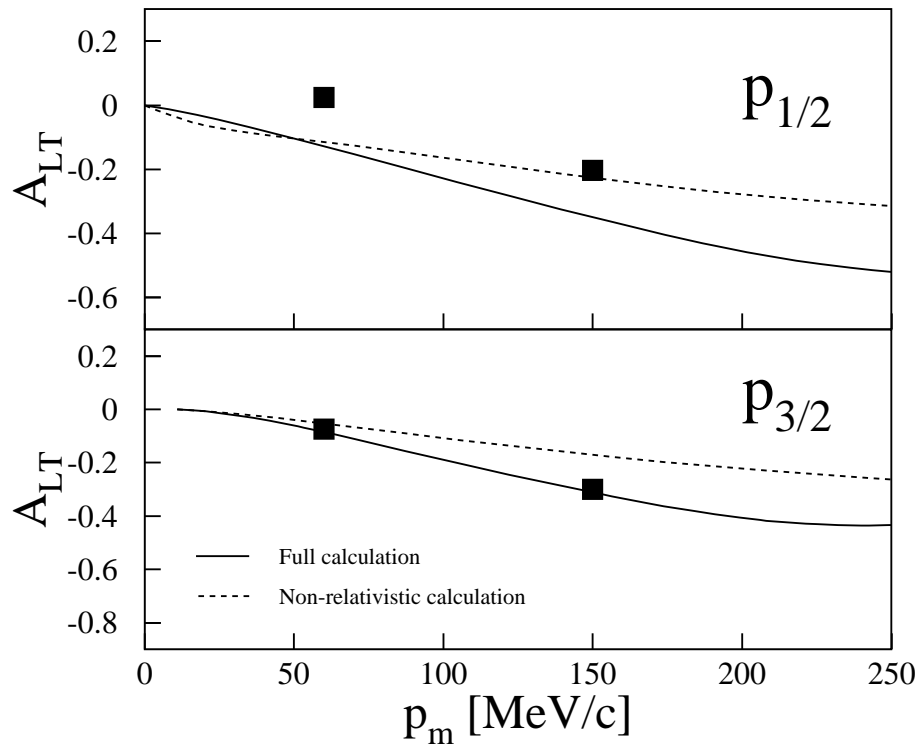


Figure 10

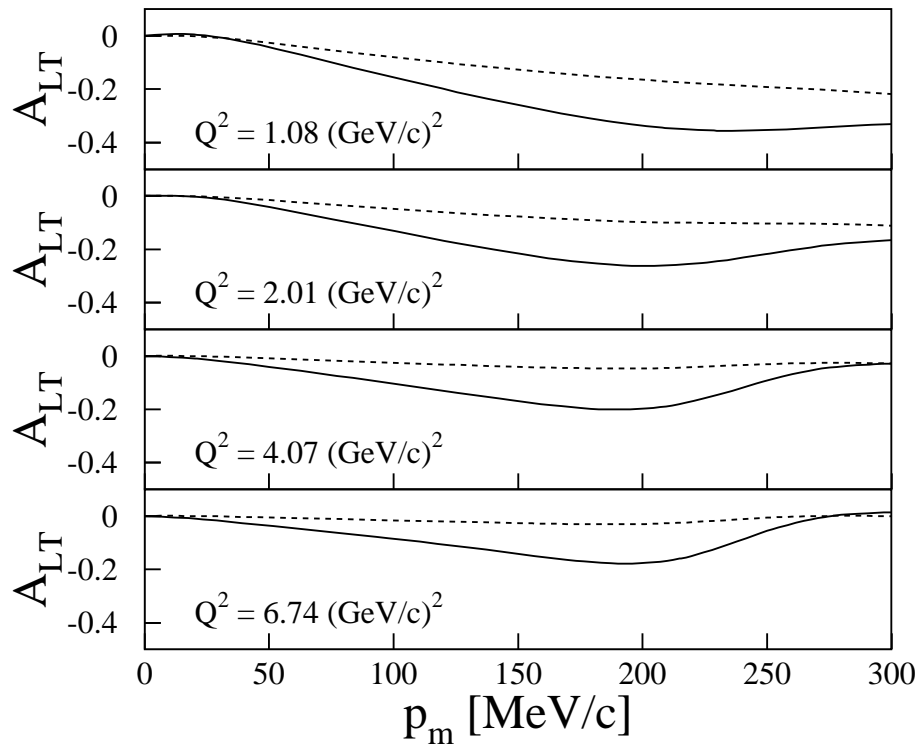


Figure 11